IEICE TRANS. ELECTRON., VOL.E100–C, NO.11 NOVEMBER 2017

INVITED PAPER *Special Section on Electronic Displays*

Comparison of Divergence Angle of Retro-Reflectors and Sharpness with Aerial Imaging by Retro-Reflection (AIRR)*

Norikazu KAWAGISHI[†,††a)], **Kenta ONUKI**[†], ***and*** **Hirotsugu YAMAMOTO**[†,†††], ***Nonmembers***

SUMMARY This paper reports on the relationships between the performance of retro-reflectors and the sharpness of an aerial image formed with aerial imaging by retro-reflection (AIRR). We have measured the retro-reflector divergence angle and evaluated aerial image sharpness by use of the contrast-transfer function. It is found that the divergence angle of the retro-reflected light is strongly related to the sharpness of the aerial image formed with AIRR.

key words: *aerial image, retro-reflector, divergence angle, sharpness, contrast transfer function*

1. Introduction

Recently, a variety of techniques to form a floating aerial image have attracted attention from the industrial world. When an aerial image is formed as a real image, the aerial image satisfies multiple cues, including binocular parallax, motion parallax, accommodation, and convergence. Thus, an aerial real image has been considered to cause less visual fatigue and be highly safe. Imaging with passive optics is a typical technique which forms such an aerial real image. For example, an aerial image is formed by use of a dihedral corner reflector array (DCRA) [1], a crossed slit-mirror array called an AI plate [2], and a retro-reflector. The DCRA and the AI plate both form an aerial image after double reflections, while single reflected light causes undesired pseudo images that locate on the both side of the aerial image. Furthermore, they require challenging and high-cost manufacturing processes for precise fabrication. We have proposed a method of aerial imaging by retro-reflection (AIRR) [3], [4]. AIRR consists of simple, mass-production, and cost-effective optical elements. Furthermore, AIRR features a wide view angle of more than 120 degrees, and solves the problem of pseudo images as mentioned above. However, AIRR has problems of low brightness and image blur. A method to improve the brightness of an aerial image formed with AIRR, which we call polarized AIRR (p-AIRR), has been realized through polarization modulations [5]–[7]. Brightness and image quality of an aerial image formed with AIRR are greatly affected by the optical properties of the retro-reflector. Thus, investigation of a retro-reflector is one of the important factors to improve aerial image quality. We have also evaluated the reflectance properties such as the reflectance and polarization maintenance ratio of retro-reflective materials [6], [7].

The purpose of this paper is to investigate the relationships between the divergence angle of retro-reflectors and the contrast transfer function (CTF) of aerial image formed with AIRR. Under condition of a fixed floating distance, aerial images of test patterns with different spatial frequencies are recorded with a camera. Performance of a retro-reflector for AIRR is shown in a CTF curve. Although the optical properties of the retro-reflective material have been reported [8], [9], the spread of retro-reflected light by commercially available retro-reflectors has not been reported. Therefore, the influence on the aerial image quality is not clear. In this paper, we clarify the divergence angle of the retro-reflected light strongly relates to the sharpness of the aerial image. Although earlier version of this work has already been reported [10], [11], this paper describes details of experiments and deeper analysis.

2. Aerial Imaging by Retro-Reflection (AIRR)

2.1 Type of Retro-Reflective Material

The main function of retro-reflective material is to reflect light back along its incident direction. Retro-reflecting sheeting is widely used for traffic signs in order to improve visual recognition at night. Photographs and features of typical retro-reflectors are shown in Fig. 1 and Table 1. There are two types of retro-reflective materials: bead type and prism type. Bead type, shown in Fig. 1 (a), is consisted of many small glass beads. The size of each glass bead is approximately in the range of 40 to 90 μm in diameter. Light is refracted by the bead surface. Then, the light is reflected by the mirror that is coated on the backside of the bead, refracted again by the bead surface, and returns to the light source. On the other hand, prism type, shown in Fig. 1 (b), consists of small corner-cube prisms. The size of each prism is approximately in the range of 100 to 200 μm. Light is reflected sequentially by the three sides of a prism and finally returns to the light source. It has been generally recognized that the prism type has a higher reflective performance

Manuscript received February 27, 2017.
Manuscript revised June 2, 2017.

[†]The authors are with Utsunomiya University, Utsunomiya-shi, 321–8585 Japan.
[††]The author is with Yazaki Corporation, Susono-shi, 410–1194 Japan.
[†††]The author is with JST, ACCEL, Utsunomiya-shi, 321–8585 Japan.

*An earlier version of this paper was presented at The 23rd International Display Workshops.

a) E-mail: norikazu.kawagishi@jp.yazaki.com

DOI: 10.1587/transele.E100.C.958

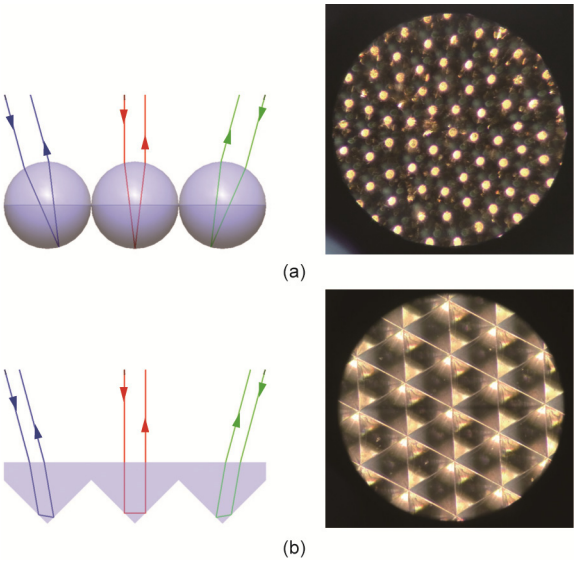

Fig. 1 Compositions of retro-reflector of (a) beads type and (b) prism type.

Table 1 Feature of retro-reflective material.

	Beads type	Prism type
Reflectance	High	Very high
Viewing angle	Wide	Narrow
Shape	Flexible	Only flat

compared with the beads type. The viewing angle of the bead type, however, is much wider than that of the prism type. Note that the viewing angle of a retro-reflector means the range of incident angle of light that is retro-reflected. In this paper, we evaluate commercially available retro-reflective sheets without logos because they are suitable for AIRR.

2.2 Principle of AIRR

Imaging by retro-reflection was originally proposed to correct a pseudoscopic image [12]. We have utilized a retro-reflector to form aerial information display. The fundamental structure of our proposed aerial display is shown in Fig. 2. The setup consists of a light source, a beam splitter, and a retro-reflector. Light rays from the light source impinge on the beam splitter. Then, rays reflected by the beam splitter impinge on the retro-reflector. After retro-reflection, the rays travel back along their incident directions. Rays that transmit through the beam splitter converge in the air. Thus, the aerial image of the light source is formed at the plane symmetrical position of the light source regarding the beam splitter. Optical loss is caused by the light transmitted through the beam splitter from the light source and the light reflected on the beam splitter after retro-reflection. Consequently, challenges of AIRR are to improve the brightness and image quality.

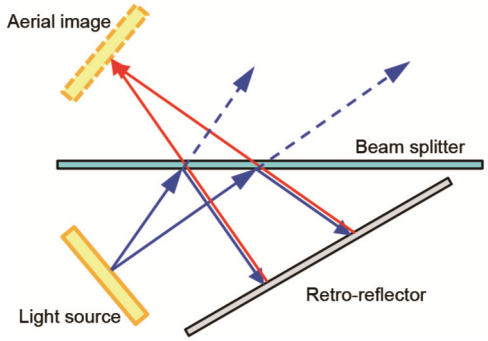

Fig. 2 Principle of aerial imaging by retro-reflection (AIRR).

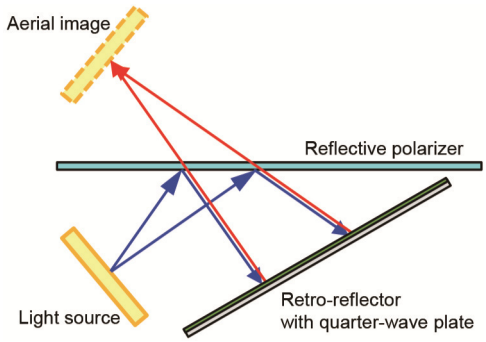

Fig. 3 Principle of polarized AIRR (p-AIRR).

2.3 Principle of Polarized AIRR (p-AIRR)

The principle of polarized AIRR is shown in Fig. 3. A polarization modulation technique has been introduced to improve the brightness of AIRR. Polarized AIRR employs a reflective polarizer instead of a beam splitter and a quarter-wave plate on the retro-reflector. Theoretically, the linearly polarized light reflected by the reflective polarizer is converted to circularly polarized light through the quarter-wave plate when the angle between the slow axis and the axis of linearly polarized light is 45 degrees. Then, the circularly polarized lights reflected by the retro-reflector is converted to linearly polarized light oriented at 90 degrees after the light passes through the quarter-wave plate again. Thus, optical loss is decreased by controlling the polarization state. The brightness of an aerial image with p-AIRR is expected to be twice that of conventional AIRR.

3. Divergence Angle of Retro-Reflectors

3.1 Optical System to Measure the Divergence Angle of a Retro-Reflector

The optical system to measure the divergence angle of a retro-reflector is constructed in this paper. A schematic diagram of our optical system to measure divergence angle is shown in Fig. 4. A screen is placed at the focal plane of a convex lens. A collimated beam from a laser passes through

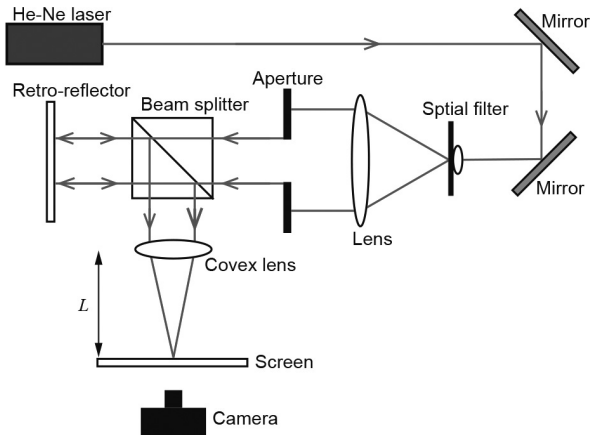

Fig. 4 Optical system to measure divergence angle of a retro-reflector.

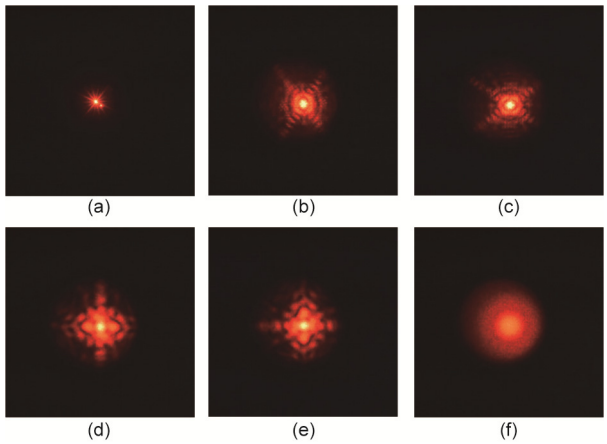

Fig. 5 Photographs of the screen on which retro-reflected light was projected. (a) Mirror. (b) Longitudinal Nikkalite CRG. (c) Lateral Nikkalite CRG. (d) Longitudinal ReflexiteHA42. (e) Lateral Reflexite HA42. (f) 3M scotchlite 8910.

the beam splitter and is reflected by a retro-reflector. The reflected light is focused by the convex lens and is projected on the screen. The light projected on the screen is affected by scattering and diffraction, which are due to retro-reflector structures. The projected pattern is recorded by a camera. The divergence angle of the retro-reflector is calculated from the recorded image. The formula to obtain the divergence angle θ of a retro-reflector is given as follows:

$$\theta = 2\tan^{-1}\frac{D}{L}, \tag{1}$$

where D is the beam diameter of the spotlight projected on the screen, and L is the focal length of the convex lens.

3.2 Experiment Measuring the Divergence Angle of Retro-Reflectors

In this experiment, we have investigated four prism-type retro-reflectors, which are longitudinal Nippon Carbide Nikkalite CRG, lateral Nippon Carbide Nikkalite CRG, longitudinal Reflexite HA42, and lateral Reflexite HA42. We have also examined a bead type, which is 3M scotchlite 8910. We compared the divergence angle of these five retro-reflectors and a mirror as a reference. The light source is a He-Ne laser (7 mW, 632.8 nm). The distance L from the convex lens to the screen is 200 mm. The recording conditions of the camera are ISO 400, 1/50 second exposure, and F-number 4.5.

Figure 5 shows photographs of the projected patterns on the screen. The divergence distribution of reflected light depends on the type of retro-reflective material. The divergence distributions of the prism types are anisotropic. On the other hand, the bead type shows an isotropic pattern. Figure 6 shows the divergence angle of the examined retro-reflectors which are calculated according to Eq. (1).

In the examined retro-reflectors, Nikkalite CRG, which is a prism type, provides the smallest divergence angle. 3M scotchlite 8910, which is a bead type, shows the largest divergence angle. The beam diameter projected on the screen is 0.8 mm with the reference mirror. In the horizontal direction, the divergence width of Nikkalite CRG is 1.8 mm, that

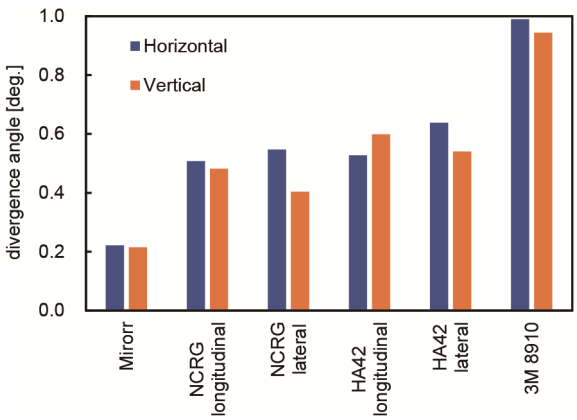

Fig. 6 Divergence angle of retro-reflectors.

is, the divergence angle is 0.51 degrees. 3M scotchlite 8910 gives a spread width of 3.5 mm, that is, the divergence angle is 0.99 degrees. Thus, the divergence angles of these retro-reflectors have nearly twice the performance difference.

4. Contrast Transfer Function of Aerial Images

4.1 Method to Evaluate Aerial Image Quality

We have proposed a method to evaluate aerial image quality, which employs contrast transfer function (CTF) [10]. A schematic diagram of our optical system to obtain CTF of an aerial image is shown in Fig. 7. This optical system consists of a light source, a test chart, a beam splitter, and a retro-reflector. The test chart is a negative 1951 USAF resolution test chart. The aerial image of the test chart is recorded with a camera. Sharpness for each spatial frequency is calculated on the recorded aerial image.

A conceptual diagram of calculating the CTF is shown in Fig. 8. The maximum intensity value I_{max} and the minimum intensity value I_{min} on the recorded aerial image are

measured for each spatial frequency. The contrast $C(x)$ at a spatial frequency x is obtained by

$$C(x) = \frac{I_{\max} - I_{\min}}{I_{\max} + I_{\min}}. \quad (2)$$

The contrast transfer function $CTF(x)$ is obtained by normalizing the contrast $C(x)$ obtained at each spatial frequency with the contrast $C(0)$ of the lowest spatial frequency in the test pattern. Thus, $CTF(x)$ is expressed by

$$CTF(x) = \frac{C(x)}{C(0)}. \quad (3)$$

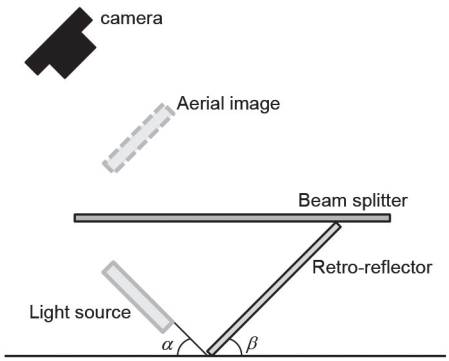

Fig. 7 Optical setup to measure sharpness of aerial image.

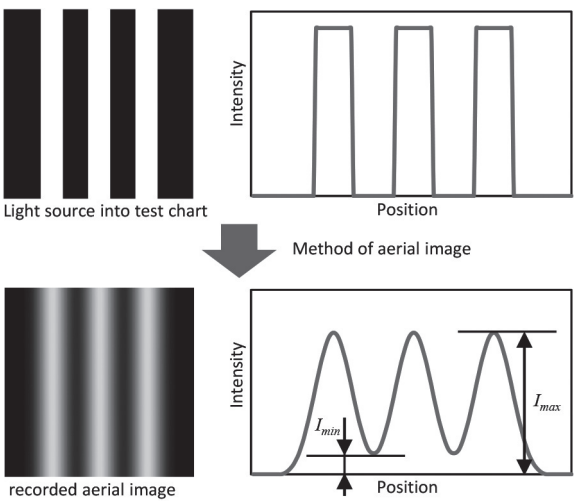

Fig. 8 Conceptual diagram of calculating CTF.

4.2 Experimental Results

In this experiment, we used two prism-type retro-reflectors (lateral Nippon Carbide Nikkalite CRG and longitudinal Reflexite HA42) and a bead-type retro-reflector (3M scotchlite 8910). As a light source, we used a white screen of a smartphone (Sony Xperia Z3 Tablet Compact). The test chart is a negative 1951 USAF resolution test chart (Thorlabs R3L3S1N). Installation angle α of the light source and installation angle β of the retro-reflector, shown in Fig. 7, were 40 degrees and 50 degrees, respectively. The beam splitter is a half mirror (transmittance and reflectance are close to 50%). We use a digital camera (Nikon, D7100). The recording conditions of the camera are ISO 800, 1/25 second exposure time, and F-number 5.6. Its 35-mm equivalent focal length is 50 mm.

The recorded aerial images are shown in Fig. 9. The effect of the retro-reflector on the CTF of the formed aerial image has been examined. Figure 10 shows several typical examples of intensity distribution in the vertical direction in a domain in Fig. 9. The maximum and minimum intensity values obtained from each spatial frequency domain as shown in Fig. 9 are calculated. CTF curves that were obtained according to Eqs. (2) and (3) are shown in Fig. 11. The spatial resolution of the prism type is more than twice as high as that of the bead type. Nikkalite CRG gives the highest spatial resolution among the three types of retro-reflectors used in the experiments.

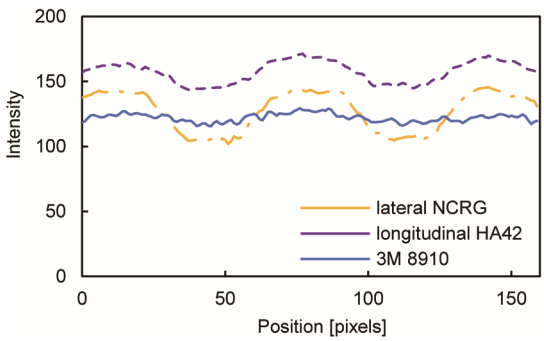

Fig. 10 Examples of profile of intensity in the vertical direction in a domain in the test chart in Fig. 9.

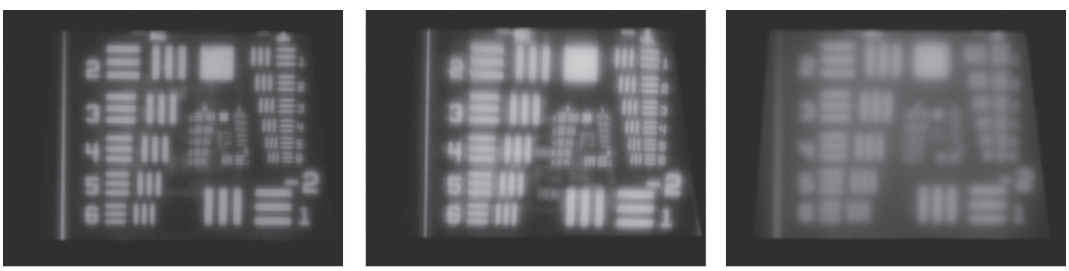

Fig. 9 Recorded aerial image that is formed by use of (a) Lateral Nikkalite CRG, (b) Longitudinal ReflexiteHA42, and (c) 3M scotchlite 8910.

4.3 Measurement of the Contrast Transfer Function When F-Number is Varied

The effect of F-number on evaluating CTF of an aerial image is illustrated in Fig. 12. It has been generally recognized that the sharpness of a photographed image of a blurred aerial image improves as F-number increases. Thus, we have investigated dependence of CTF on F-number. The aerial image is recorded while varying the F-number of the camera from F4.2 to F8.0. Experimental conditions other than F-number are the same as those in Sect. 4.2. In the case of the retro-reflector of lateral Nikkalite CRG, the recorded aerial images with different F-numbers are shown in Fig. 13. Figure 14 shows CTF curves obtained according to Eqs. (2) and (3). Of the three F-numbers, F8.0 gives the highest spatial resolution, and F4.2 gives the lowest. Results show that sharpness of aerial image is affected by F-number.

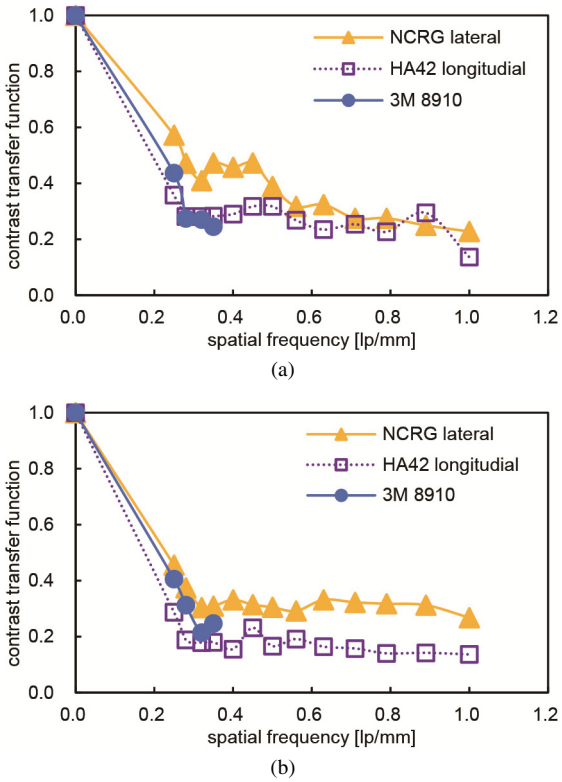

Fig. 11 Results on CTF of aerial images in (a) horizontal direction, (b) vertical direction.

4.4 Measurement of Contrast Transfer Function Under a Fixed Floating Distance Condition

In Fig. 11 and Fig. 14, there are some fluctuations in the CTF curves obtained with the USAF test target. One of the reasons for this may be the variation in the distance of bar patterns in the test target from a retro-reflector because image blur of the aerial image in AIRR depends on the floating distance. Therefore, it is necessary to evaluate image quality under condition of a fixed floating distance. Therefore, we use a test chart shown on a light source display instead of a USAF test target in this section.

Experimental results in Sect. 3 show that the divergence angle of the retro-reflected light varies depending on the installing direction of the retro-reflector. It is suggested that CTF changes according to the installing direction of a retro-reflector. In this experiment, we investigate five retro-reflectors (longitudinal Nikkalite CRG, lateral Nikkalite CRG, longitudinal Reflexite HA42, lateral Reflexite HA42, and 3M scotchlite 8910). We measure the sharpness of aerial images formed by use of these retro-reflectors. The light source is a TFT LCD display (Litemax Electronics, SLD0868). Installation angles α and β, shown in Fig. 7, are both 45 degrees. The beam splitter is a half mir-

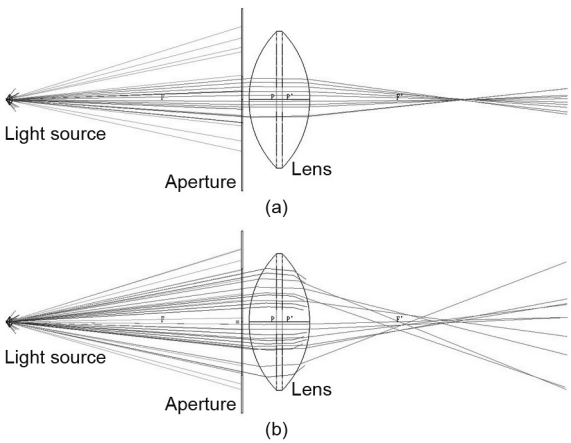

Fig. 12 Ray tracing examples to show effect of F-number on the point spread function (a) with large F-number and (b) with small F-number.

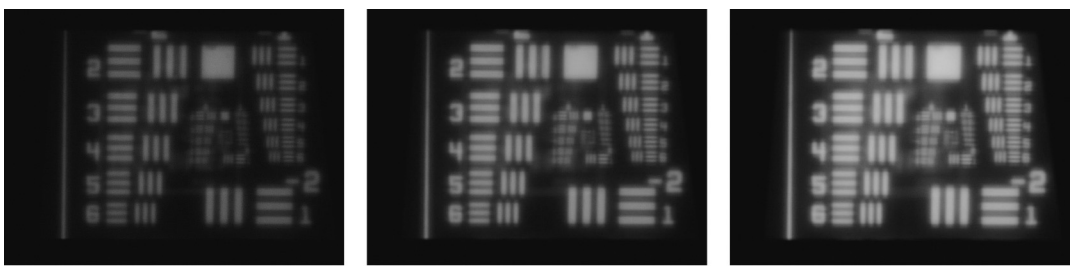

Fig. 13 Recorded aerial images with F-number (a) F8.0, (a) F5.6, and (c) F4.2.

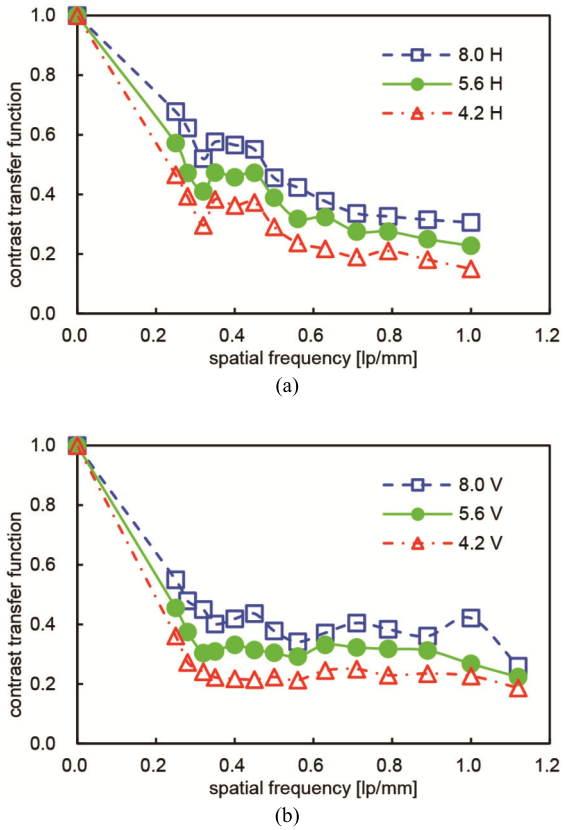

Fig. 14 CTF curves of aerial images recorded with different F-numbers in (a) horizontal direction and (b) vertical direction.

ror (transmittance and reflectance are close to 50%). We use a digital camera (Nikon, D5500). The recording conditions of the camera are ISO 400, 1/80 second exposure time, and F-number 4.5. Its 35mm equivalent focal length is 50 mm.

Examples of the aerial images are shown in Fig. 15. The retro-reflectors of prism type formed finer images than that of bead type.

The horizontal CTF curves obtained from the aerial images are shown in Fig. 16. Results show that Nikkalite CRG, which is of prism type, forms an aerial image in the best contrast. On the other hand, lateral Reflexite HA42 and 3M scotchlite 8910 form an aerial image in low contrast. The vertical CTF curves obtained from the aerial images are shown in Fig. 17. Results show that longitudinal Nikkalite CRG forms an aerial image in the best contrast. On the other hand, longitudinal Reflexite HA42 and 3M scotchlite 8910 form an aerial image in low contrast. For the reasons mentioned above, Nikkalite CRG forms an aerial image in the most excellent contrast under the measured spatial frequency range.

The CTF curves shown in Figs. 16 and 17 change smoothly while the CTF curves in Fig. 14 and Fig. 15 are wavy. This difference suggests that CTF curves were influenced by floating distance. By using this digital test target pattern, we have obtained a more accurate CTF curve than the conventional method that used a fixed USAF test target. Sharpness of the aerial image is an important factor for selecting a retro-reflector for AIRR. However, there is no standard method for evaluating the sharpness of an aerial image now. Our proposed method can be a common evaluation method of many other aerial imaging techniques.

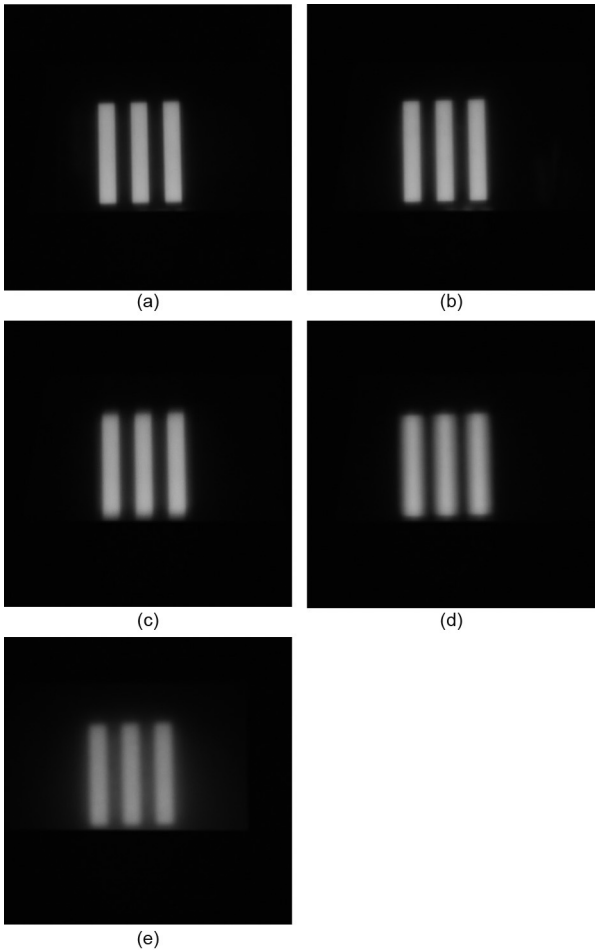

Fig. 15 Photograph of aerial image that is formed with AIRR by use of (a) longitudinal Nikkalite CRG, (b) lateral Nikkalite CRG, (c) longitudinal Reflexite HA42, (d) lateral Reflexite HA42, and (e) 3M scotchlite 8910.

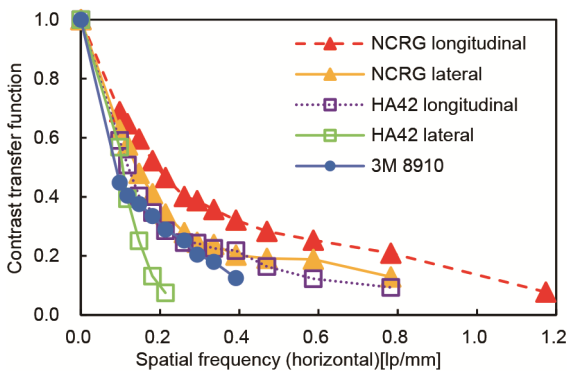

Fig. 16 Results on CTF of aerial images in the horizontal direction.

5. Conclusion

We have investigated the relationship between the diver-

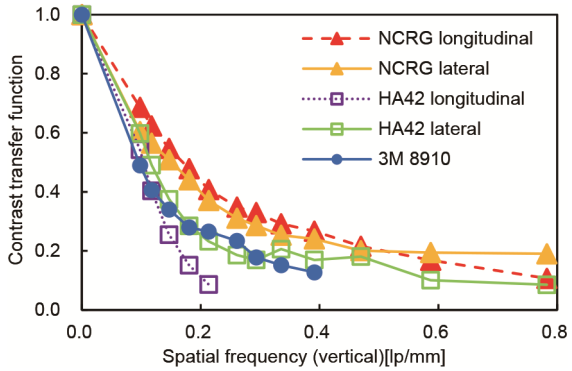

Fig. 17 Results on CTF of aerial images in the vertical direction.

gence angle of retro-reflectors for AIRR and the contrast transfer function (CTF) of an aerial image formed by use of retro-reflector with AIRR. It was found that the divergence angle of the retro-reflected light strongly relates to the sharpness of the aerial image. Evaluating the retro-reflective material showed the possibility to predict the image quality of the aerial image without forming an aerial image. Furthermore, our proposed method can be a common evaluation method of many other aerial imaging techniques with dihedral corner reflector array and slit-mirror array.

Acknowledgements

The authors with to thank Dr. Nathan Hagen who assisted in the proof-reading of the revised manuscript.

References

[1] S. Maekawa, K. Nitta, and O. Matoba, "Transmissive optical imaging device with micromirror array," Proc. SPIE, vol.6392, Three-Dimensional TV, Video, and Display V, 63920E, Oct. 2006.
[2] Asukanet, "Aerial imaging technologies," http://aerialimaging.tv/, accessed Feb. 13, 2017.
[3] H. Yamamoto and S. Suyama, "Aerial 3D LED display by use of retroreflective sheeting," Proc. SPIE 8648, Stereoscopic Displays and Applications XXIV, 86480, San Francisco, Feb. 2013.
[4] H. Yamamoto, Y. Tomiyama, and S. Suyama, "Floating aerial LED signage based on aerial imaging by retro-reflection (AIRR)," Opt. Express, vol.22, no.22, pp.26919–26924, Nov. 2014. DOI:10.1364/OE.22.026919
[5] Y. Tokuda, A. Hiyama, M. Hirose, and T. Large, "Comparison of material combinations for bright and clear floating image by retro-reflective re-imaging technique," Proc. of The 21th International Display Workshops, no.3D2-3L, pp.818–819, Niigata, Japan, Dec. 2014.
[6] M. Nakajima, Y. Tomiyama, I. Amimori, and H. Yamamoto, "Evaluation methods of retro-reflector for polarized aerial imaging by retro-reflection," Proc. CLEO-PR 2015, no.25B1-2, Busan, Korea, Aug. 2015.
[7] M. Nakajima, K. Onuki, I. Amimori, and H. Yamamoto, "Polarization state analysis for polarized aerial imaging by retro-reflection (PAIRR)," Proc. of The 22th International Display Workshops, no.FMC5-3, pp.429–432, Otsu, Japan, Dec. 2015.
[8] Y. Tan and H. Chen, "Diffraction of transmission light through triangular apertures in array of retro-reflective microprisms," Appl. Opt., vol.51, no.16, pp.3403–3409, June 2012. DOI:10.1364/AO.51.003403
[9] D.C. O'Brien, G.E. Faulkner, and D.J. Edwards, "Optical properties of a retroreflecting sheet," Appl. Opt., vol.38, no.19, pp.4137–4144, July 1999. DOI:10.1364/AO.38.004137
[10] N. Kawagishi and H. Yamamoto, "Evaluation method of sharpness on aerial image formed with AIRR," Proc. of The 22th International Display Workshops, no.3D6-1, pp.826–829, Otsu, Japan, Dec. 2015.
[11] K. Onuki, N. Kawagishi, and H. Yamamoto, "Comparison of divergence angle of retro-reflectors for aerial imaging by retro-reflection (AIRR)," Proc. of The 23th International Display Workshops, no.FMCp1-5, pp.542–545, Fukuoka, Japan, Dec. 2016.
[12] C.B. Burckhardt, R.J. Colloer, and E.T. Doherty, "Formation and inversion of pseudoscopic Images," Appl. Opt., vol.7, no.4, pp.627–631, April 1968. DOI:10.1364/AO.7.000627

Norikazu Kawagishi received his B.E. and M.E. degrees in Systems Engineering from Wakayama University in 2005 and 2007, respectively. He worked at NEC Display Solutions Ltd. during 2007 to 2014. He moved to Yazaki Corporation in 2014. He joined a graduate school of Engineering (doctor's course), Utsunomiya University in 2015. He is now with Yazaki Research and Technology Center, Yazaki Corporation. He is interested in information display and human machine interface.

Kenta Onuki received his B.E. degrees from Utsunomiya University in 2016. Currently, he is a graduate student in Dept. of Optical Engineering at Utsunomiya University. His research interests include aerial display systems and reflection characteristics of retro-reflector. He is a member of The Japan Society of Applied Physics (JSAP) and The Optical Society (OSA).

Hirotsugu Yamamoto was born in Wakayama, Japan, in 1971. He received his B.E., M.E., and Ph.D. degrees from the University of Tokyo. From 1996 to 2008, he was an assistant professor at Tokushima University. From 2009 to 2014, he was an associate professor at Tokushima University. Since 2014, he has been an associate professor at Utsunomiya University. His recent work activities have included aerial display, digital signage by use of high-speed LED panels, 3D display, secure display, and information photonics for emerging information communications technologies. Dr. Yamamoto was a recipient of Young Scientist Award for the Presentation of an Excellent Paper, The Japan Society of Applied Physics, Outstanding Poster Paper Award at IDW'03, IDW'04, IDW'07, IDW'08, IDW'09, IDW'10, IDW'11, IDW'12, IDW'13, IMID2014, IDW'14, IMID2015, IDW'15, IMID2016, and IDW'16, Best Paper Award at DHIP2011, IDW'11, and IDW'15, Best 3D Demonstration Award at Stereoscopic Displays and Applications 2012, and the Gen-Nai Grand Prize from the Ozaki Foundation of Japan.